DES of Flow Past an Oscillating Cylinder Located Downstream of Backward-facing Step

H. S. Park[1] and B. Thornber[1]

[1]School of Aerospace, Mechanical and Mechatronic Engineering
University of Sydney, New South Wales 2006, Australia

Abstract

Flow past a transversely oscillating circular cylinder located in the downstream region of a backward-facing step is numerically studied as foundational work for the simulation of flow around a helicopter fuselage in its landing and launching operation on board a ship. In the present study, Detached Eddy Simulation (DES) with the incompressible flow at high Reynolds number is conducted using OpenFOAM. The geometry has its basis on Simplified Frigate Shape (SFS) by the fact that the backward-facing step resembles the hangar, and vertically oscillating cylinder describes the unsteady motion of the aircraft fuselage in station-keeping flight. Changes in wake field due to the interaction with downstream of the backward-facing step and the wall layer have been observed. In addition, two different approaches to deal with the boundary of a cylinder are studied: the immersed boundary (IB) method and fully-resolved boundary layer, in the laminar flow over a stationary cylinder case without the step for the consideration of a future application to the current research. A quantitative comparison is made between both approaches of handling boundaries.

Introduction

Flow past a cylinder has been a traditional research subject of fluid dynamics as the flow field facilitates a variety of complex phenomena such as geometry-dependent vortex flow in the wake region, flow separation in the boundary layer, and flow transition from laminar to turbulent, despite its geometrical simplicity [1]. Another famous classic problem is the flow over a backward-facing step, which has been extensively studied for several decades. This simple geometry is of particular interest to investigate separated flows and its reattachment followed by recirculation and recovery.

In this paper, flow past an oscillating circular cylinder located in the downstream region of a backward-facing step, which combines the two traditional problems described above, is studied at $\mathrm{Re_D} = 1.4 \times 10^5$ (based on the cylinder diameter D and freestream velocity U_∞). The case setup is designed as preparatory work for the future study on the coupled flow of ship airwake and rotor-induced flow, which appears in the ship-helicopter dynamic interface (DI) operation, around the fuselage. CFD simulation of the DI operation has been explored for many years as part of an effort to reduce the number of at-sea trials, accurately define ship-helicopter operating limits, and consider its results in ship design [2]. The DI operation on or near the helideck of a ship is known for its extremely challenging environment mainly due to the turbulent airwake generated by the superstructure and hangar of a ship. Despite a number of complex flow aspects in the DI operation, the problem is simplified from understanding that the flow can be regarded similar to that for a backward-facing step and the fuselage, namely the cylinder, in recirculation region close to the rear face of the hangar due to the confined space of the flight deck [3]. It is hence expected that this simplified three-dimensional simulation of shipboard helicopter operation will provide an important background for further investigation.

This work also includes a comparative study of two different approaches to cope with the boundary of cylinder: the IB method and fully-resolved boundary layer. The IB method was initially introduced by Peskin [4] to study blood flow in the cardiovascular system and is now expanded to a number of modifications. The IB method uses momentum forcing in the Navier-Stokes equation rather than a real body conforming grid, providing significant advantages to memory and CPU savings by allowing much simpler grids, such as Cartesian mesh, for simulations. It becomes more potent for moving bodies since the computation does not need to regenerate grid in every time step [5]. For these reasons, the IB method is expected to be an excellent remedy for future application to the ship-helicopter DI simulation by saving computational cost which appears highly expensive due to the geometrical complexity of objects and mesh regeneration to reflect their movements.

The primary challenge in developing IB algorithm is the imposition of the boundary condition (BC) on the IB [6]. In general, two main approaches in the IB method are utilised to deal with this challenge. They are called continuous forcing approach and discrete forcing approach, respectively. The main difference between them is when to apply the forcing to the momentum equation, where the former incorporates the forcing into the continuous governing equation before discretisation, whereas the latter does after discretisation. The main focus of the present work is on the discrete forcing approach since the application of the continuous forcing approach for solid boundaries is limited only to low Reynolds number flows [6]. The discrete forcing approach is also subdivided into two ways of BC imposition: indirect and direct. The indirect BC imposition employs a spreading step using smooth delta function to transform the forcing field onto the underlying mesh. On the other hand, the boundary reconstruction is carried out in the direct BC imposition, by assigning the forcing only to the nearest cells of the IB which is calculated from their surrounding cell values and the BC directly applied onto the IB.

At present, both indirect and direct BC impositions of the discrete forcing approach based on the finite volume method are available within OpenFOAM [7, 8]. Hence, both libraries are tested with the flow past a fixed cylinder at low Reynolds number to study a capability of the IB method by comparison against the wall-resolved approach and existing references.

Numerical Methods

Navier-Stokes Solver

The Navier-Stokes equation and the continuity equation for unsteady incompressible viscous fluid are written with forcing term **f** as:

$$\frac{\partial \mathbf{u}}{\partial t} + \mathbf{u} \cdot \nabla \mathbf{u} = \nu \nabla^2 \mathbf{u} - \rho^{-1} \nabla p + \mathbf{f} \qquad (1)$$

$$\nabla \cdot \mathbf{u} = 0 \qquad (2)$$

where **u** is velocity, p is pressure, ν and ρ are kinematic viscosity and density, respectively.

Two different simulations are performed at $\text{Re}_\text{D} = 100$ and 1.4×10^5 in this study. Segregated solver with PISO (Pressure Implicit with Separation of Operators) algorithm [9] is used to solve pressure-velocity coupling in both cases. The standard PISO solver provided in OpenFOAM is modified for use of each library as instructed in [7, 8], and employed for the low Reynolds number simulation.

Second-order implicit scheme is used for spatial discretisation in both cases. For temporal discretisaion, first-order implicit Euler scheme is applied in $\text{Re}_\text{D} = 100$ case for accurate comparison with the outcomes in [7]. Second-order implicit Crank-Nicolson scheme is employed for time-stepping in $\text{Re}_\text{D} = 1.4 \times 10^5$ simulation.

For high Reynolds number case, DES with Spalar-Allmaras (SA) turbulence model [10] is conducted to capture unsteady flow structure. Thus the kinematic viscosity ν in Eq.(1) is replaced by an effective viscosity $\nu_\text{eff} = \nu + \nu_t$. In SA turbulence model, the modified turbulent viscosity $\tilde{\nu}$ is introduced and its transport equation is solved to determine the turbulent viscosity ν_t. Spalding's formula [12] is used for near-wall treatment.

Computational Domain

Computational domain used for $\text{Re}_\text{D} = 100$ case is a rectangular with $[-20D, 40D] \times [-20D, 20D]$ in x, y direction, respectively. The number of cells is fixed to be 155,000. Grid spacing in circumferential area $[-1D, 1D] \times [-1D, 1D]$ of the domain for IB cases is set to be $0.01D$. The first cell distance of wall-resolved case is determined as $0.01D$, accordingly. The same set of BCs in [7] is adopted.
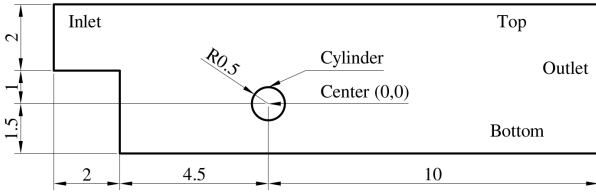
Figure 1: Computational domain for the flow over an oscillating cylinder located downstream of a backward-facing step. All dimensions are normalised based on the diameter of cylinder.

For $\text{Re}_\text{D} = 1.4 \times 10^5$ case, the domain in Figure 1 with $\sim 1.25M$ cells is used for simulation. Spanwise length is chosen to be $5D$ and discretised by 100 cells. The step height $2.5D$ is selected to secure enough space for the cylinder to oscillate at the amplitude $A = 0.25D$ with the frequency ratio $f_o/f_v = 1$, where f_o and f_v are the frequency of the simple harmonic cross-flow oscillation and the vortex shedding frequency in a fixed cylinder case without the step at $\text{Re}_\text{D} = 1.4 \times 10^5$, respectively. The distance $4.5D$ from the vertical wall to the centre of the cylinder is arbitrarily chosen to be enough to see the effect of recirculation on the cylinder, considering the scaled distance between the rear face of hangar and the middle of helideck in SFS, based on the step height. Since the simulation is to look at the flow field in an atmospheric environment, free slip condition is used for the top boundary, unlike usual backward-facing step simulations. Inlet and outlet conditions are the same as those in $\text{Re}_\text{D} = 100$ case. The bottom is considered as a wall, whereas front and back are chosen to be periodic.

Immersed Boundary Method

The indirect BC imposition of the discrete forcing approach in OpenFOAM employs the research work in [11]. The uniqueness of this approach is that a kernel function in a polynomial basis is used to deal with the different types of back-ground mesh, not limited to the equidistant Cartesian mesh. A brief workflow is introduced below, and details can be found in [7, 11]. The library used in this study is distributed on 21/02/18.

The singular force $\mathbf{F}^*$ on k-th Lagrangian point at n-th time step is obtained from the velocity value $\mathbf{U}$ on its boundary Γ and the velocity field $I(\mathbf{u}^*)$ interpolated onto the IB:

$$\mathbf{F}^* \left(\mathbf{X}_k, t^n \right) = \frac{\mathbf{U}^\Gamma \left(\mathbf{X}_k, t^n \right) - I \left(\mathbf{u}^* \right)}{\Delta t} \tag{3}$$

where $\mathbf{u}^*$ is the predicted velocity. The interpolation operator I is defined as:

$$I \left[\mathbf{u}^* \right] = \sum_{j \in D_k} \mathbf{u}_j \tilde{w}_d \left(\mathbf{x}_j - \mathbf{X}_k \right) \Delta v \tag{4}$$

where j-index stands for the discrete value of the velocity field, and D_k refers to the support cage domain centred on the k-th Lagrangian point. The support is designed to identify at least three Eulerian nodes in each direction for calculations, involved with the localised window function $\tilde{w}_d$. Δv is the volume of the cell centred at $\mathbf{x}_j$. The singular force field defined over Γ is reflected onto the Eulerian field by a spreading operator C as:

$$\begin{aligned}
\mathbf{f}^* \left(\mathbf{x}_j, t^n \right) &= C \left[\mathbf{F}^* \left(\mathbf{X}_k, t^n \right) \right] \\
&= \sum_{k \in D_j} \mathbf{F}^* \left(\mathbf{X}_k, t^n \right) \tilde{w}_d \left(\mathbf{x}_j - \mathbf{X}_k \right) \epsilon_k
\end{aligned} \tag{5}$$

where D_j refers to the support containing the j-th Eulerian node. ϵ_k is the Lagrangian quadrature [7].

Lastly, the discretised momentum equation in implicit form is solved with the forcing:

$$\frac{\mathbf{u}^* - \mathbf{u}^n}{\Delta t} = -H \left(\mathbf{u}^n, \mathbf{u}^{n-1} \right) - G p^n + \frac{1}{\text{Re}} L \left(\mathbf{u}^*, \mathbf{u}^n \right) + \mathbf{f}^* \tag{6}$$

where H is the discrete advection operator, G and L are the discrete gradient and Laplacian, respectively.

In the direct BC imposition of the discrete forcing approach, on the other hand, the BC is involved with the solver directly assigning to a band of cells after interpolation, the equations not being solved with the entire forcing field. Dependent variable values at each centre of cells nearest to the boundary are updated at every boundary correction stage. The values are calculated by quadratic interpolation with the weighted least square method [8]. The library used in the present work is included in `foam-extend-4.0`.

For two-dimensional case, Dirichlet BC is given by:

$$\begin{aligned}
\phi_p = \phi_{ib} &+ C_0 \left(x_p - x_{ib} \right) + C_1 \left(y_p - y_{ib} \right) \\
&+ C_2 \left(x_p - x_{ib} \right) \left(y_p - y_{ib} \right) \\
&+ C_3 \left(x_p - x_{ib} \right)^2 + C_4 \left(y_p - y_{ib} \right)^2
\end{aligned} \tag{7}$$

where p and ib, respectively, stand for the cell centre of interest and the relevant point on the IB. Neumann BC defined in a local coordinate system $x'y'$ with x'-axis being normal to a given point on IB and y'-axis being tangent to the point is written as:

$$\begin{aligned}
\phi_p = C_0 \left[\vec{n}_{ib} \cdot (\nabla \phi) \right] x'_p &+ C_1 y'_p + C_2 x'_p y'_p \\
&+ C_3 \left(x'_p \right)^2 + C_4 \left(y'_p \right)^2
\end{aligned} \tag{8}$$

All the unknown coefficients involved above are evaluated by the weighted least square method.

Result

Flow over a fixed cylinder at $Re_D = 100$

Simulation results of the stationary cylinder case without the backward facing step at $Re_D = 100$ are summarised in Table 1. The computation is carried out for 50 cycles in terms of a vortex shedding period, and the values of the last 20 cycles are used to obtain the outcomes. The mean separation angle ($\bar{\theta}_s$) is taken from the average of 20 samples over an entire shedding period.

	$\bar{C}_D$	C'_L	St	$\bar{\theta}_s$
Present				
Wall-resolved	1.35	0.33	0.167	117.3
Indirect BC	1.38	0.33	0.167	115.3
Direct BC	1.34	0.33	0.167	118.7
Numerical				
Kim et al. [5]	1.33	0.32	0.165	-
Constant et al. [7]	1.37	-	0.165	118.9
Blackburn and Henderson [13]	1.35	-	-	
Experimental				
Williamson [14]	-	-	0.164	-
Wu et al. [15]	-	-	0.164	117.4

Table 1: Simulation results with data from literature for flow past a fixed cylinder at $Re_D = 100$.

The results obtained from IB methods in Table 1 are in a good agreement with both numerical and experimental data, where $\bar{C}_D$ is the time-averaged drag coefficient, C'_L and St are the amplitude of the lift coefficient and Strouhal number, respectively. Primarily, the original work of indirect BC imposition [7] is adequately reproduced within a range.
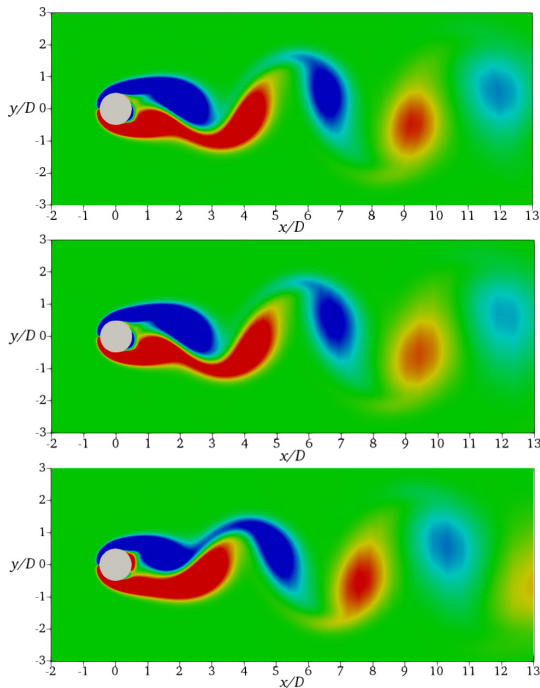
Figure 2: Vorticity contours at $Re_D = 100$ within a range of $-U_\infty/D \sim U_\infty D$. Wall-resolved case(top), indirect BC case(middle), and direct BC case(bottom) at the same instant.

One interesting point is the wall-clock time spent for each simulation. Figure 3 shows the error in terms of the mean drag coefficient against the wall-clock time measured using a single core as the grid is refined. From this comparison, the conventional wall-resolved method is found to be the most computationally efficient, whereas the direct BC imposition shows superior performances to the indirect BC imposition in both computational cost and accuracy. The reason why the indirect BC imposition is the slowest is that the momentum equation has to be solved twice, where the first step is to provide a predicted velocity field for the interpolation of forcing and the second is to obtain another predicted velocity field for the pressure equation with the BC on the IB considered.
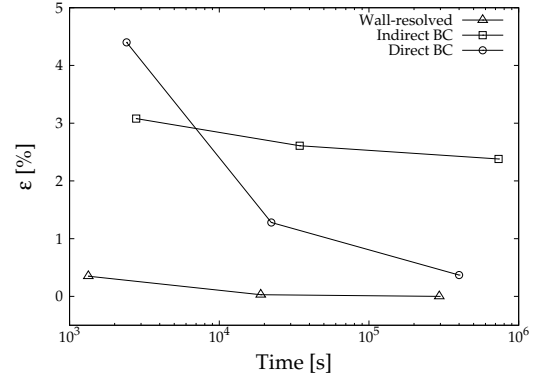
Figure 3: Grid refinement study of wall-resolved method and both IB methods with the error in terms of mean drag coefficient and wall-clock time instead of grid spacing in $Re_D = 100$ simulation.

Flow past an oscillating cylinder at $Re_D = 1.4 \times 10^5$

For the fair discussion of this simulation, the flow over a fixed cylinder is additionally studied as well as the flow past an oscillating cylinder. Time-dependent results of the lift and drag coefficients are presented in Figure 4.
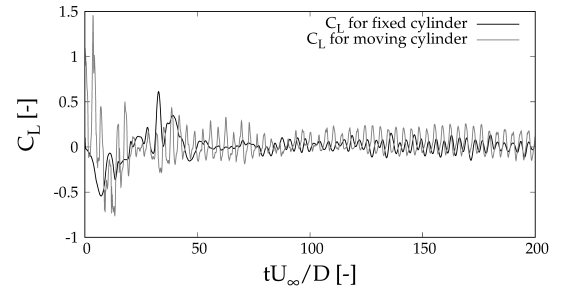
(a) Lift coefficient for a fixed and an oscillating cylinder
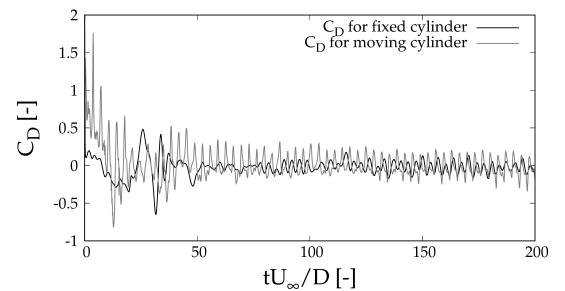
(b) Drag coefficient for a fixed and an oscillating cylinder

Figure 4: Time-dependent results at $Re_D = 1.4 \times 10^5$.

Force coefficients for both fixed and moving cylinders show a similar manner in oscillation at steady-state, while those for a moving cylinder have relatively larger amplitude. Time-averaged values of the coefficients in both cases are close to zero, whereas the flow over a fixed cylinder case without the step at the same Reynolds number has the mean drag coefficient within $0.6 \sim 0.8$ due to flow separation [1]. The reason why force coefficients in this case shows such a periodic behaviour is that the cylinder is in the recirculation zone, the strong vertical flow dominates the flow around the cylinder and it periodically circulates along its boundary. Figure 5 well describes the circulating flows and the bluff body wake influenced by the separated flow from the step in the ascending motion of the cylinder. The unsteady flow in spanwise direction is another different aspect incurred by the flow over the step, as presented in Figure 6.
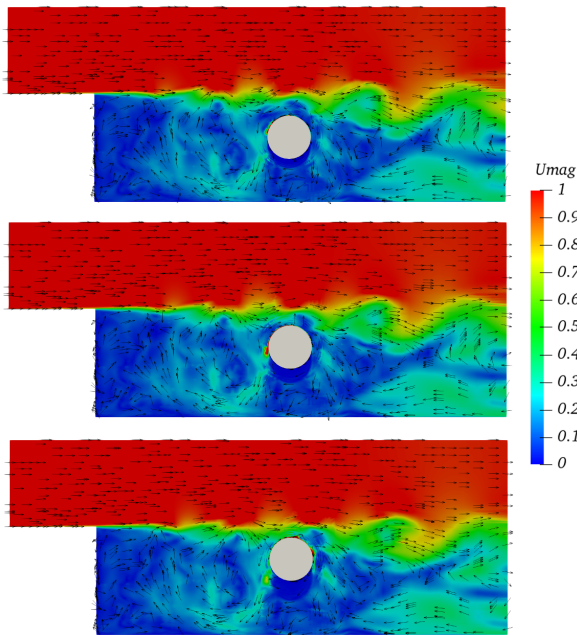
Figure 5: Elevation view of velocity contour coloured by normalised velocity magnitude and velocity vector plots in ascending motion at $\mathrm{Re_D} = 1.4 \times 10^5$. $y = 0$ (top), $y = 1/2A$ (middle), and $y = A$ (bottom), where $y = 0$ is the vertical location of the cylinder centre at $t = T$.
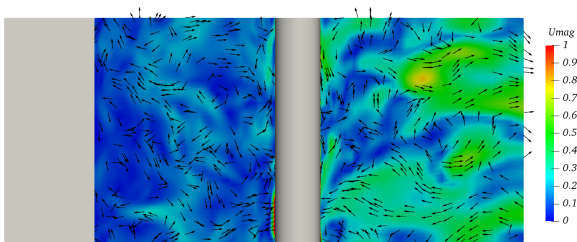
Figure 6: Instantaneous plan view of velocity contour coloured by its magnitude and velocity vector plots at $\mathrm{Re_D} = 1.4 \times 10^5$.

Conclusions

In the present study, two IB methods in OpenFOAM are investigated using the low Reynolds number flow over a fixed cylinder simulation. The results from both indirect and direct BC imposition of the IB method are well agreed with not only those obtained from the wall-resolved method but referenced data from the literature. The direct BC imposition is found to be more computationally efficient and accurate than the other,

so the future application of the IB method based on the direct BC imposition for the ship-helicopter DI simulation is considered to be a better choice. Furthermore, high Reynolds number flow over an oscillating cylinder in the downstream region of a backward-facing step is studied. From the lift and drag on the cylinder and the qualitative results, it could be found that the circulating flow dominates the flow around the cylinder and it strongly affects the dynamics of the cylinder.

References

[1] Lo, S.-C., Hoffmann, K.A. and Dietiker J.-F., Numerical Investigation of High Reynolds Number Flows over Square and Circular Cylinders, *J. Thermophys Heat Transfer*, **19**, 2005, 72–80.

[2] Linton, D., Thornber, B. and Widjaja, R., A Study of LES Methods for Simulation of Ship Airwakes, In *46th AIAA Fluid Dynamics Conference*, AIAA Aviation, 2016.

[3] Lee, R. and Zan, S.J., Wind Tunnel Testing of a Helicopter Fuselage and Rotor in a Ship Airwake, *J. Am. Helicopter Soc.*, **50**, 2005, 326–337.

[4] Peskin, C.S., Flow Patterns around Heart Valves: A Numerical Method, *J. Comput. Phys.*, **10**, 1972, 252–271.

[5] Kim, J., Kim, D. and Choi, H., An Immersed-Boundary Finite-Volume Method for Simulations of Flow in Complex Geometries, *J. Comput. Phys.*, **171**, 2001, 132–150.

[6] Mittal, R. and Iaccarino, G., Immersed Boundary Methods, *Annu. Rev. Fluid Mech.*, **37**, 2005, 239–261.

[7] Constant, E., Favier, J., Meldi, M., Meliga, P. and Serre, E., An Immersed Boundary Method in OpenFOAM: Verification and Validation, *Comput. Fluids*, **157**, 2017, 55–72.

[8] Jasak, H., Rigler, D. and Tuković, Ž., Design and Implementation of Immersed Boundary Method with Discrete Forcing Approach for Boundary Conditions, *6th European Conference on Computational Fluid Dynamics - ECFD VI*, 2014.

[9] Issa, R., Solution of the Implicitly Discretised Fluid Flow Equations by Operator-Splitting, *J. Comput. Phys.*, **62**, 1986, 40–65.

[10] Spalart, P.R., Jou, W.-H., Strelets, M. and Allmaras, S.R., Comments on the feasibility of LES for wings, and on a hybrid RANS/LES approach, *1st AFOSR Int. Conf. on DNS/LES*, 1997.

[11] Pinelli, A., Naqavi, I.Z., Piomelli, U. and Favier, J., Immersed-Boundary Methods for General Finite-Difference and Finite-Volume Navier-Stokes Solvers, *J. Comput. Phys.*, **229**, 2010, 9073–9091.

[12] Spalding, D.B, A Single Formula for the "Law of the Wall", *J. Appl. Mech.*, **28**, 1961, 455–458.

[13] Blackburn, H. and Henderson, R., A Study of Two-Dimensional Flow Past an Oscillating Cylinder, *J. Fluid. Mech.*, **385**, 1999, 255–286.

[14] Williamson, C.H.K., Vortex Dynamics in the Cylinder Wake, *Annu. Rev. Fluid. Mech.*, **28**, 1996, 477–539.

[15] Wu, M.H., Wen, C.Y., Yen, R.H., Weng, M.C. and Wang, A.B., Experimental and Numerical Study of the Separation Angle for Flow Around a Circular Cylinder at Low Reynolds Number, *J. Fluid. Mech.*, **515**, 2004, 233–260.